Structural and functional analysis of SET8, a histone H4 Lys-20 methyltransferase

Jean-François Couture,[1] Evys Collazo,[1] Joseph S. Brunzelle,[2] and Raymond C. Trievel[1,3]

[1]Department of Biological Chemistry, University of Michigan, Ann Arbor, Michigan 48109, USA; [2]Life Sciences Collaborative Access Team, Advanced Photon Source, Argonne National Laboratory, Argonne, Illinois 60439, USA

SET8 (also known as PR-SET7) is a histone H4-Lys-20-specific methyltransferase that is implicated in cell-cycle-dependent transcriptional silencing and mitotic regulation in metazoans. Herein we report the crystal structure of human SET8 (hSET8) bound to a histone H4 peptide bearing Lys-20 and the product cofactor S-adenosylhomocysteine. Histone H4 intercalates in the substrate-binding cleft as an extended parallel β-strand. Residues preceding Lys-20 in H4 engage in an extensive array of salt bridge, hydrogen bond, and van der Waals interactions with hSET8, while the C-terminal residues bind through predominantly hydrophobic interactions. Mutational analysis of both the substrate-binding cleft and histone H4 reveals that interactions with residues in the N and C termini of the H4 peptide are critical for conferring substrate specificity. Finally, analysis of the product specificity indicates that hSET8 is a monomethylase, consistent with its role in the maintenance of Lys-20 monomethylation during cell division.

Nucleosomes are the fundamental unit of packaging of DNA in eukaryotes and are composed of 146 bp of DNA wound around a histone octamer comprised of two copies each of the core histones H2A, H2B, H3, and H4. In the presence of linker histones, such as H1, nucleosomes can be arranged into higher-ordered structures, further compacting the DNA and creating a repressive environment that silences transcription. Both core and linker histones undergo a myriad of post-translational modifications that govern numerous genomic functions, including transcription, mitosis, DNA repair, and recombination (Fischle et al. 2003). Site-specific methylation of lysines, which occurs within histones H1, H3, and H4, has recently emerged as an important modification in the epigenetic control of gene expression (Sims et al. 2003; Kuzmichev et al. 2004). Methylation of Lys-20 in histone H4 is unique among these sites because of its involvement in a diverse array of nuclear processes. Lys-20 methylation is enriched in transcriptionally silent regions (Fang et al. 2002; Nishioka et al. 2002), and trimethylation of this lysine selectively marks pericentric heterochromatin (Schotta et al. 2004). In addition, this modification has been linked to mitotic regulation in

metazoans (Julien and Herr 2004; Karachentsev et al. 2005), cellular aging in mammals (Sarg et al. 2002), and DNA damage checkpoint control in the cell cycle of *Schizosaccharomyces pombe* (Sanders et al. 2004).

Research by various groups has resulted in the identification of several histone H4 Lys-20-specific protein methyltransferases (PKMTs), including metazoan SET8 (also known as PR-SET7) (Fang et al. 2002; Nishioka et al. 2002), *Drosophila* ASH1 (Beisel et al. 2002), murine NSD1 (Rayasam et al. 2003), and mammalian SUV4-20H1/2 (Schotta et al. 2004) and its *Schizosaccharomyces pombe* ortholog SET9 (Sanders et al. 2004). These enzymes are members of the SET domain methyltransferase family that catalyze the methylation of select lysines in proteins using the cofactor S-adenosylmethionine (AdoMet) (Trievel 2004). SET8 is the most studied of the Lys-20-specific PKMTs and has been shown to function in transcriptional silencing in metazoans (Rice et al. 2002). Expression of this PKMT fluctuates during the cell cycle and peaks during the G2/M transition. During M phase, SET8 becomes phosphorylated (Georgi et al. 2002) and is recruited to mitotic chromosomes (Rice et al. 2002). Both the expression and localization of SET8 coincide with global fluctuations in the level of Lys-20 methylation during the cell cycle, which peaks during mitosis. The resulting Lys-20 methylation pattern can be maintained beyond a single round of cell division, suggesting that SET8 propagates an epigenetic

imprint in transcriptional silencing (Rice et al. 2002; Karachentsev et al. 2005).

In addition to cell-cycle-dependent gene silencing, this PKMT also plays a pivotal role in mitotic regulation in metazoans. In *Drosophila*, loss-of-function mutations in the *SET8* gene result in lethality during the larval to pupal transition in development (Nishioka et al. 2002; Karachentsev et al. 2005). An analysis of the *SET8* mutants reveals a significant decrease in histone H4 Lys-20 mono-, di-, and trimethylation in comparison to the chromatin of wild-type larvae and correlates with a general loss in heterochromatic silencing (Karachentsev et al. 2005). Larvae with *SET8*-null mutations also exhibit abnormalities in mitosis that result in reduced cell size and multinucleation, implying that the cells have undergone endoreplicative cell division. Similar phenomena have been observed when SET8 expression is perturbed in HeLa cell lines (Julien and Herr 2004). RNA interference of the gene encoding HCF-1 (herpes simplex virus host cell factor-1), a transcription factor that regulates the expression of SET8, disrupts proper expression of the enzyme, resulting in altered levels of monomethyl-Lys-20 during mitosis. These aberrations coincide with severe mitotic defects including improper chromosome segregation during metaphase, aberrant cytokinesis, and multinucleated daughter cells, correlating with the effects of the *SET8*-null mutants in *Drosophila*. Taken together, these studies firmly establish that SET8 has a critical role in mitotic regulation in metazoans through maintenance of Lys-20 monomethylation during cell division.

To gain greater insights into the biological functions of this enzyme, we have determined the crystal structure of human SET8 (hSET8) bound to a histone H4 peptide bearing Lys-20 and the product cofactor S-adenosylhomocysteine (AdoHcy). The structure of the ternary complex and the accompanying biochemical analysis reveal the mechanism by which hSET8 specifically recognizes Lys-20 in H4. In addition, the structure elucidates a novel interaction between the cofactor and histone H4 that is not observed in other SET-domain PKMTs. Finally, product specificity analysis indicates that hSET8 is a bona fide histone H4 Lys-20 monomethylase, correlating with its functions in transcriptional silencing and maintaining Lys-20 monomethylation during mitosis.

Results and Discussion

Overall structure of the hSET8 ternary complex

To elucidate the structure of hSET8 in complex with histone H4, we cocrystallized a construct of the enzyme encoding the catalytic SET domain (residues 191–352) with a 10-residue H4 peptide (A-K-R-H-R-K_{20}-V-L-R-D) and the product AdoHcy. Removal of the N-terminal 190 residues was necessary in order to obtain diffraction-quality crystals of the complex, but did not impair the activity of the enzyme (see below). The structure was determined at 2.0 Å resolution by selenomethionyl multiple wavelength anomalous dispersion (MAD) phasing

using an I220M mutant to enhance the Se anomalous signal (Fig. 1A). The experimentally phased structure was then used as a molecular replacement model to determine the structure of the wild-type hSET8 in complex with the histone H4 peptide and AdoHcy at 1.45 Å resolution (Table 1).

The overall fold of the catalytic domain of hSET8 is structurally conserved with other SET-domain PKMTs (Trievel 2004). The SET domain is composed of a single-turn 3_{10} helix (3_{10-1}) and 12 β-strands (β1–β12) arranged into four antiparallel β-sheets and a single parallel β-sheet (Fig. 1B; Trievel et al. 2002). An α-helix (α2) is inserted between the β5- and β6-strands of the SET domain, as is observed in the structures of the histone H3 methyltransferases *Neurospora* DIM-5 (Zhang et al. 2002) and human SET7/9 (Wilson et al. 2002). This helix
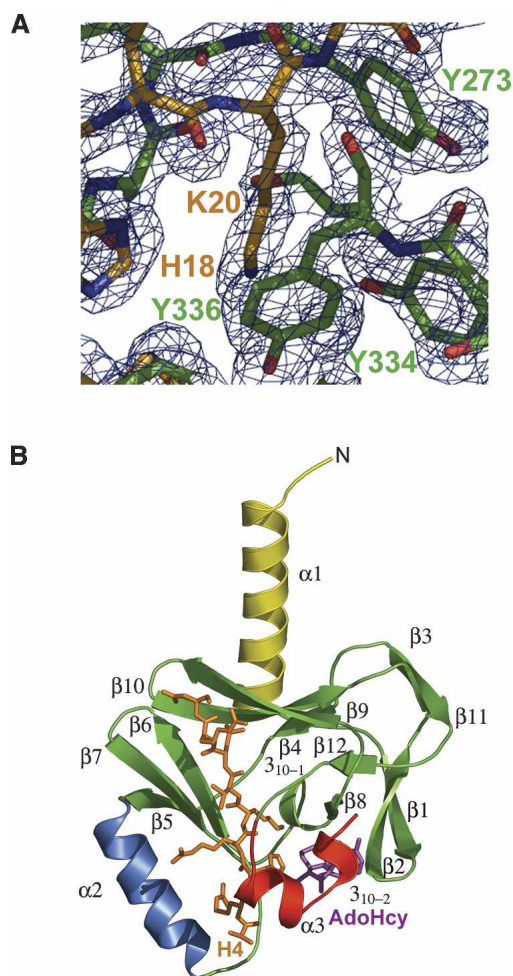

Figure 1. Crystal structure of hSET8. (*A*) Experimental Se-MAD phased electron density map at 2.0 Å resolution illustrating the active site of hSET8 bound to Lys-20 in histone H4. The map is contoured at 1.0 σ. The carbon atoms of hSET8 and the histone H4 residues are displayed and labeled in green and gold, respectively. (*B*) Ribbon diagram of the secondary structure of hSET8 with the β-strands and α- and 3_{10}-helices denoted. The SET, nSET, iSET, and cSET regions are depicted in green, yellow, blue, and red, respectively, while AdoHcy and the H4 peptide are represented in magenta and orange, respectively.

Table 1. *Data and refinement statistics for the crystal structure of hSET8 bound to AdoHcy and a histone H4 peptide*

Data collection	Native	Se-Met data of I220M mutant		
		Inflection	High remote	Peak
Space group: P1	a = 43.9, b = 45.7, c = 94.4	a = 44.3, b = 44.7, c = 52.3		
	$\alpha = 89.2$, $\beta = 87.1$, $\gamma = 90.7$	$\alpha = 64.8$, $\beta = 88.8$, $\gamma = 89.5$		
Wavelength (Å)	0.9686	0.9792	0.9686	0.9791
Resolution (Å)	1.45	2.0	2.0	2.0
R_{merge} (%)	4.2 (19.2)[a]	4.7 (7.2)	5.1 (5.9)	6.4 (8.7)
$I/\sigma I$	19.48 (6.9)	22.5 (19.7)	21.5 (20.0)	12.5 (9.8)
Reflections				
Total	405,744	96,027	95,740	68,780
Unique	122,436	23,246	24,153	24,087
Completeness	94.1 (90.1)	95.1 (87.2)	95.5 (91.5)	95.2 (94.9)
Phasing power		3.615	3.589	2.879
Sites found/Total				6/8
F.O.M.[b]				0.8328

Refinement (native)		R.M.S.	
Resolution Range	10–1.45 Å	Bond length (Å)	0.008
Reflections (Fo > 2σ)	405,744	Bond angles (°)	1.188
Final Model		B-factors (Å^2)	16.15
Protein atoms	5132		
H4/AdoHcy	304/114	Average B-factors (Å^2)	
Water atoms	1007	Protein	14.37
R-factors[c]		Histone H4/AdoHcy	15.27/8.16
$R_{working}$	16.9	Water	26.22
R_{free}	19.9		

[a]Numbers in parentheses refer to data in the highest resolution shell.
[b]After phasing in SHARP.
[c]R-factor: $R_{working} = \sum || Fo | - | Fc || / \sum | Fo |$; $R_{free} = \sum T || Fo | - | Fc || / \sum T | Fo |$, where T is a test data set consisting of 5% of the total reflections randomly chosen and set aside before refinement.

forms the inserted SET or iSET region, and variations in the sequence and structure of this motif play a key role in determining the substrate specificity of different PKMTs (Xiao et al. 2003b). In contrast, the N- and C-terminal regions that flank the SET domain of hSET8 (referred to as the nSET and cSET regions, respectively) are not conserved in the structures of other histone methyltransferases. In the nSET region, a single α-helix (α1) precedes the SET domain, similar to the N-terminal α-helix of Rubisco large subunit methyltransferase (LSMT), a plant SET-domain enzyme (Trievel et al. 2002). The cSET region of hSET8 is composed of a short α-helix (α3) and a 3_{10} helix (3_{10-2}) that pack against the cofactor and protein substrate-binding sites. Mutations within this region abrogate substrate binding and catalysis (see below), agreeing with the truncation studies reported by Zhang and colleagues (Fang et al. 2002).

AdoMet-binding site

The product AdoHcy adopts a horseshoe-shaped conformation in the cofactor-binding pocket that is formed by the β1–β2 turn, the loop preceding β6, the β8-strand, and the α3-helix in the cSET region (Fig. 1B). The adenine moiety of AdoHcy is sandwiched between the indole ring of Trp-349 and the aliphatic side chain of Lys-226,

and the purine N6 and N7 atoms hydrogen-bond to the backbone carbonyl and amide groups of His-299, respectively (Fig. 2A). At the opposite end of the cofactor, the positively charged α-amino group is recognized by a trigonal array of hydrogen bonds with the main chain carbonyl oxygens of Lys-226 and Arg-228 and the amide Oδ of Asn-298. In addition, the carboxylate moiety of the AdoHcy forms a highly conserved salt-bridge interaction with the guanidinium group of Arg-228 and also hydrogen-bonds to the hydroxyl of Tyr-271. Overall, the cofactor-binding mode is structurally conserved with other SET-domain methyltransferases and serves to orient the methyl group of AdoMet into the methyltransfer pore during catalysis (Trievel 2004).

Despite these similarities, a striking difference is observed in the interactions with the ribose moiety of AdoHcy in the hSET8 ternary complex. In the structures of other SET-domain PKMTs, the ribose hydroxyls of the cofactor are either solvent-exposed, such as in hSET7/9 (Xiao et al. 2003a) and Rubisco LSMT (Trievel et al. 2002), or hydrogen-bonded with neighboring residues, as is observed in DIM-5 (Zhang et al. 2003). However in the hSET8 ternary complex, the 3'-OH hydroxyl engages in a direct hydrogen bond with the imidazole moiety of His-18 in the histone H4 peptide (Fig. 2A). This novel substrate–cofactor interaction does not occur within other
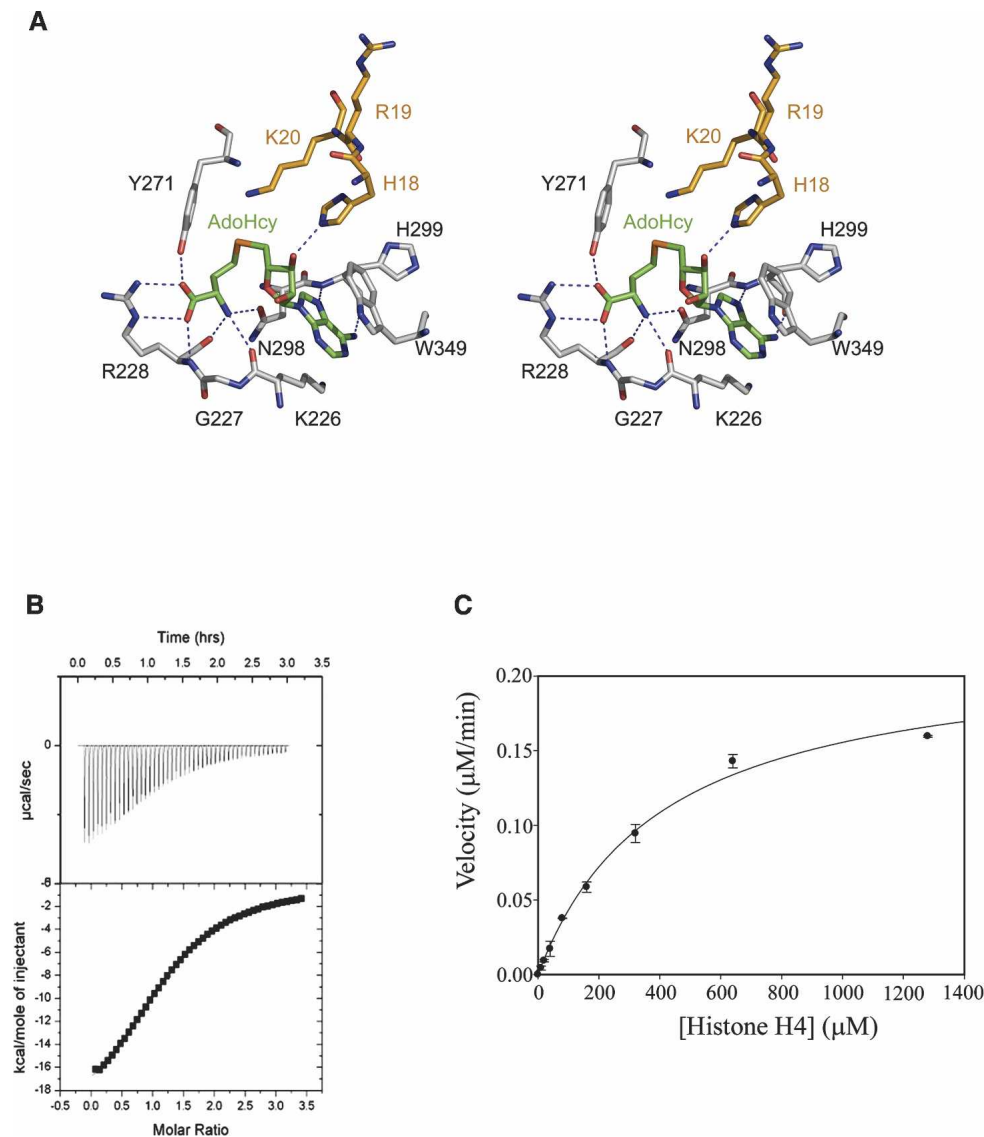
Figure 2. Cofactor-binding pocket. (*A*) Stereoview of the cofactor-binding cavity in complex with AdoHcy. The carbon atoms in hSET8, the cofactor, and the H4 peptide are depicted in gray, green, and gold, respectively. Hydrogen bonds are illustrated as dashed blue lines. (*B*) ITC titration experiment with the wild-type histone H4 peptide and hSET8 (*upper* trace) and the fitted binding curve (*lower* trace). (*C*) Michaelis-Menten plot of the initial velocity versus substrate concentration for the methylation of the H4 peptide by hSET8.

SET-domain enzymes because the residues that line the floor of the protein substrate-binding cleft occlude the AdoMet-binding pocket, preventing direct contact between the histone and the cofactor. Using isothermal titration calorimetry (ITC) (Fig. 2B), we determined that mutation of His-18 to phenylalanine modestly affects the affinity of hSET8 for histone H4, whereas substitution of this residue by alanine (H18A) completely abolishes binding (Table 2). Interestingly, both the H18F and H18A substitutions severely abrogate AdoHcy binding (J.-F. Couture and R.C. Trievel, unpubl.), suggesting that the hydrogen bond between His-18 and the cofactor is important for high-affinity binding of AdoMet. However, steady-state kinetic analysis of native hSET8 (Fig. 2C)

and the His-18 mutants reveals that the H18F mutant exhibits only a slight reduction in its substrate specificity (k_{cat}/K_M value) in comparison to the native H4 peptide, while the H18A mutant completely eliminates histone H4 methylation by hSET8. Collectively, these results suggest that the hydrogen bond between the cofactor and His-18 in histone H4 enhances the affinity of AdoMet for hSET8, but is not essential for catalysis.

Histone H4 recognition by hSET8

The experimental map obtained from the Se-MAD phasing of hSET8 yielded unambiguous electron density for residues 16–24 in histone H4. The H4 peptide binds in a

Table 2. *Mutational analysis of histone H4 and the substrate binding cleft of hSET8*

hSET8	K_D (μM)	K_M (μM)	k_{cat} (min^{-1})	k_{cat}/K_M (μM^{-1} × min^{-1}) × 10^3
Wild type	33 ± 1	400 ± 30	0.43 ± 0.02	1.1 ± 0.1
E259A	>500	—	—	0.06 ± 0.01
E259Q	84 ± 2	870 ± 7	0.12 ± 0.01	0.14 ± 0.01
C270A	>500	—	—	0.09 ± 0.02
D338A	>500	N.A.	N.A.	N.A.
D338N	>500	N.A.	N.A.	N.A.
H347A	>500	1020 ± 40	0.20 ± 0.04	0.20 ± 0.04
H347F	1.6 ± 0.1	7.4 ± 1.2	0.21 ± 0.01	28 ± 2
H347E	>500	470 ± 40	0.08 ± 0.01	0.17 ± 0.03
H4 peptide (A$_{15}$K$_{16}$R$_{17}$H$_{18}$R$_{19}$**K$_{20}$**V$_{21}$L$_{22}$R$_{23}$D$_{24}$)				
R17A	N.B.	N.A.	N.A.	N.A.
R17E	N.B.	N.A.	N.A.	N.A.
R17Q	>500	1980 ± 50	0.12 ± 0.01	0.06 ± 0.005
R17K	240 ± 10	1890 ± 70	0.14 ± 0.04	0.07 ± 0.002
H18A	N.B.	N.A.	N.A.	N.A.
H18F	120 ± 4	420 ± 7	0.35 ± 0.03	0.84 ± 0.07
H18E	N.B.	—	—	0.09 ± 0.008
R19A	41 ± 1	310 ± 7	0.34 ± 0.02	1.1 ± 0.1
R19E	230 ± 10	1990 ± 90	0.24 ± 0.04	0.12 ± 0.02
R19Q	88 ± 2	530 ± 9	0.28 ± 0.01	0.53 ± 0.02
R19K	39 ± 1	360 ± 4	0.39 ± 0.03	1.1 ± 0.1
V21A	16 ± 1	390 ± 10	0.11 ± 0.02	0.29 ± 0.05
V21F	54 ± 3	160 ± 6	0.35 ± 0.04	2.1 ± 0.3
L22A	N.B.	—	—	0.02 ± 0.004
L22F	31 ± 2	110 ± 2	0.36 ± 0.02	3.2 ± 0.2
R23A	27 ± 1	210 ± 5	0.36 ± 0.03	1.7 ± 0.1
R23L	3.8 ± 0.1	22 ± 1	0.40 ± 0.06	22 ± 3
R23E	27 ± 2	290 ± 20	0.26 ± 0.06	0.91 ± 0.22

(>500) A lower limit of the K_D value is reported because saturation of the enzyme with ligand could not be achieved during ITC titrations.
(N.B.) No heat of binding was detected using ITC.
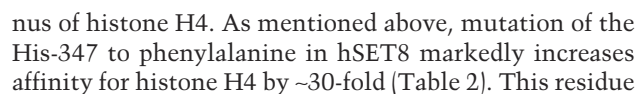(N.A.) No activity was detected in the methyltransferase assay.
(—) The individual values of K_M and k_{cat} are not reported because the K_M value is beyond the measurable range; the k_{cat}/K_M values are reported in these cases.

deep cleft formed by the β6-strand and iSET α2-helix on one side and the loop connecting the β12-strand and the cSET α3-helix on the other (Fig. 1B). To facilitate the discussion of histone H4 recognition by hSET8, we have divided the analysis of its binding into three categories based on (1) interactions with the H4 peptide backbone, (2) contacts with the side chains of residues N-terminal to Lys-20 in H4, and (3) side-chain interactions with residues C-terminal to Lys-20. The peptide backbone of histone H4 is anchored in the substrate-binding cleft through the formation of a parallel β-sheet with the β6-strand (Fig. 3A) and hydrogen-bonds with the side chains of Gln-276, Asp-338, and His-347 (Fig. 3B). Lys-20 is at the center of this β-sheet interaction, which firmly deposits the lysine side chain into the active site. A comparison of the hSET8:histone H4 complex with the structures of DIM-5 (Zhang et al. 2003) and hSET7/9 (Xiao et al. 2003a) bound to histone H3 reveals that the parallel

β-sheet-binding mode is conserved among the three PKMTs, although the substrate-binding cleft of hSET8 is deeper and more pronounced than in the other enzymes (Fig. 3A).

To probe the interactions between hSET8 and the H4 backbone, we mutated Asp-338 and His-347 and measured their effects on histone binding and methylation (Table 2). Substitution of Asp-338 to asparagine and alanine in hSET8 abolishes both histone H4 binding and methylation. The results of the asparagine mutation are surprising because its amide side chain would be expected to maintain hydrogen bonding with the backbone amide of Arg-19 in H4. However, the carboxylate of Asp-338 also hydrogen-bonds to the amide of Ser-340 in the cSET region, indicating that this residue forms a hydrogen-bond bridge between this serine and Arg-19 in H4 that cannot be maintained in the D338N mutant. Mutation of His-347 to alanine, glutamate, or phenylalanine has variable effects on the affinity and methylation of histone H4. The glutamate and alanine substitutions weaken the interactions between H4 and hSET8 as determined by ITC and also reduce the substrate specificity by approximately fivefold. In contrast, the H347F mutation enhances the affinity of hSET8 for histone H4 as judged by the decrease in the K_D and K_M values versus the wild-type enzyme, despite the loss of hydrogen bonding between the imidazole N$_\varepsilon$2 atom and the backbone carbonyl of Lys-16 in H4 (see below).

The side chains of the residues in the N-terminal part of the histone H4 peptide are recognized through an intimate series of hydrogen-bond, salt-bridge, and van der Waals interactions in the substrate-binding cleft of hSET8 (Fig. 3B). The side chain of Arg-17 in histone H4 engages in a complex array of hydrogen bonding within the binding cleft of the enzyme. The guanidinium group hydrogen-bonds to the carbonyl oxygen of Gly-269 and forms water-mediated hydrogen bonds with the backbone amide of Tyr-271 and the carbonyl oxygens of Tyr-262 and His-18 in H4. Moreover, the Arg-17 guanidinium moiety engages in a salt-bridge interaction with the carboxylate of Glu-259 and also participates in van der Waals contacts with the sulfhydryl group of Cys-270. The side chain of His-18 in histone H4 is also involved in a variety of interactions within the substrate-binding cleft. In addition to hydrogen bonding to the ribose 3′-OH of AdoHcy, the imidazole group forms edge-to-face aromatic ring interactions with the side chains of His-347 and Trp-349 in the cSET region and also participates in van der Waals contacts with the sulfhydryl group of Cys-270. The guanidinium group of Arg-19 in H4 engages in a salt-bridge interaction with the carboxylate of Glu-259 and also forms a cation–π interaction with the phenol side chain of Tyr-274. Collectively, these interactions can be grouped into two categories that appear to be important for recognition of the histone H4 N terminus by hSET8: (1) an edge-to-face aromatic cluster comprised of His-347 and Trp-349 in the enzyme and His-18 in H4 and (2) a salt-bridge network between Arg-17 and Arg-19 in H4 that is bridged by the carboxylate of Glu-259.

Figure 3. Histone substrate-binding cleft. (*A*) Two orthogonal views of the molecular surface of the histone-binding cleft of hSET8 in which the β6-strand is denoted through the transparent surface. The H4 peptide and cofactor are rendered in orange and magenta, respectively, while the secondary structure of the enzyme is depicted as in Figure 1B. (*B*) Substrate-binding cleft of hSET8 in which the carbon atoms of the protein, the H4 peptide, and the cofactor are illustrated in gray, gold, and green, respectively. Hydrogen bonds are displayed as dashed blue lines. Protein and ligands atoms are labeled according to the color of their carbon atoms, except for mutations in hSET8 that are labeled in red.

To elucidate the determinants of the histone lysine specificity of hSET8, we screened a series of site-directed mutants in the substrate-binding cleft and the N termi- nus of histone H4. As mentioned above, mutation of the His-347 to phenylalanine in hSET8 markedly increases affinity for histone H4 by ~30-fold (Table 2). This residue

participates in the aromatic cluster with Trp-349 and His-18 in H4 (Fig. 3B), and the H347F mutant substantially enhances the edge-to-face interactions among these aromatic residues. In contrast, an alanine mutation of Cys-270, whose sulfhydryl group engages in van der Waals contacts with the imidazole group of His-18 and the guanidinium moiety of Arg-17, severely disrupts histone H4 binding and methylation. Although this residue does not directly participate in the aromatic cluster or Glu-259 salt bridge, it may serve to orient the side chains of Arg-17 and His-18 within the substrate-binding cleft. In addition to the hSET8 mutations, we mutated His-18 in histone H4 to determine its effect on the specificity of the enzyme. Interestingly, the substitution of His-18 by phenylalanine does not impact the affinity to nearly the same extent as the H347F substitution in the substrate-binding cleft. However, mutation of His-18 to alanine completely abolishes both histone H4 binding and methylation by hSET8, while a glutamate substitution at this position reduces the k_{cat}/K_M value ~12-fold (Table 2). As discussed previously, His-18 hydrogen-bonds to the ribose moiety of the cofactor, enhancing the binding of AdoMet during histone methylation. Similarly, the indole ring of Trp-349 not only participates in the edge-to-face contacts within the aromatic cluster but also engages in a π-stacking interaction with the adenine ring of the cofactor (Fig. 2A). Collectively, these interactions underscore the fundamental function of the aromatic cluster in both histone H4 and AdoMet binding.

The salt-bridge network comprised of Glu-259 in hSET8 and Arg-17 and Arg-19 in histone H4 also plays a key role in substrate recognition (Fig. 3B). An alanine mutation of Glu-259, which resides in the iSET α-helix of hSET8, eliminates this salt-bridge network and dramatically impairs histone H4 binding, emphasizing its importance in substrate specificity (Table 2). Conversely, an E259Q substitution modestly reduces histone H4 binding and methylation by hSET8, indicating that hydrogen bonding between this mutant's amide side chain and the H4 arginines can partially compensate for the loss of the ionic interactions in the salt-bridge network. To identify if Arg-17 or Arg-19 (or both) is required for histone H4 recognition by the enzyme, we mutated each of these residues to alanine, glutamate, glutamine, or lysine, respectively. Mutation of Arg-17 to alanine or glutamate completely abolishes histone H4 binding and methylation, while the lysine and glutamine substitutions retain residual activity as substrates. The results with the R17K H4 mutant were somewhat surprising because of the conservation of the positive charge, which can maintain a salt bridge with the carboxylate of Glu-259. Collectively, the Arg-17 mutations strongly suggest that its guanidinium group is specifically recognized through the salt-bridge interaction with Glu-259 and by direct and water-mediated hydrogen bonds within the substrate-binding cleft of hSET8. Whereas the Arg-17 mutants abrogate interactions between the enzyme and histone H4, substitutions of Arg-19 have little impact on either H4 binding or methylation, with the exception of the R19E mutant, which reduces affinity for the enzyme

due to its negatively charged carboxylate group. To summarize, our results reveal that the salt bridge formed between Glu-259 in hSET8 and Arg-17 in histone H4 is a prerequisite for substrate binding and methylation of Lys-20 by hSET8.

In contrast to the N-terminal part of histone H4, most of the residues C-terminal to Lys-20 are solvent-exposed and do not engage in significant interactions with hSET8 (Fig. 3B). For example, mutations of Val-21 in H4 to alanine or phenylalanine have only modest effects on substrate binding and methylation by the enzyme (Table 2). However, substitution of the neighboring Leu-22 by alanine virtually abolishes histone H4 binding and reduces the substrate specificity of the enzyme >50-fold. An inspection of the substrate-binding cleft reveals that this leucine binds in a shallow hydrophobic pocket formed by the aliphatic side chains of Thr-307, Leu-309, and Leu-318 in hSET8. Mutation of Leu-22 to a phenylalanine is readily accommodated in this position, indicating that this hydrophobic pocket is a key determinant in histone H4 recognition. The side chains of the remaining residues in the H4 peptide, Arg-23 and Asp-24, do not engage in extensive interactions within the substrate-binding cleft of the enzyme. To illustrate this, substitution of Arg-23 by alanine or glutamate has no significant effect on H4 binding and methylation. Intriguingly, an R23L mutation results in an ~10-fold increase in the affinity of hSET8 for histone H4, as judged by its K_D and K_M values. It is difficult to reconcile this observation with the solvent exposure of Arg-23 in the structure of the ternary complex. However, we hypothesize that the peptide backbone of the H4 R23L mutant may adopt a different conformation when bound to hSET8, permitting this residue to engage in hydrophobic interactions with the enzyme similar to those observed for Leu-22. Taken together, these results reveal that the C terminus of histone H4 is anchored in the substrate-binding cleft of hSET8 through a hydrophobic specificity pocket that recognizes Leu-22 or other bulky hydrophobic residues in this position.

Based on our collective biochemical and structural analyses of the histone H4 specificity of hSET8, we identify a consensus motif for substrate recognition by this PKMT: R-Ω-ζ-**K**-X-Φ (where Ω is an aromatic residue, ζ is a nonacidic residue, **K** is the methylation site, X is any residue, and Φ is a bulky hydrophobic residue) (Aasland et al. 2002). The arginine (R) and an aromatic residue (Ω) are required in the N terminus of this motif because they engage in highly specific interactions within the salt-bridge network and aromatic cluster, respectively. The methylation site **K** is preceded by any nonacidic residue (ζ), ideally a basic amino acid that can participate in a salt-bridge interaction with Glu-259 in the substrate-binding cleft. At the C terminus of the motif, a bulky hydrophobic residue (Φ) is recognized through its binding in the hydrophobic specificity pocket of the substrate-binding cleft.

A comparison of the hSET8:histone H4 complex with the histone H3-bound structures hSET7/9 and DIM-5 (which methylate Lys-4 and Lys-9 in H3, respectively)

reveals substantial differences in substrate recognition by these PKMTs. In the crystal structure of DIM-5 bound to histone H3 (Zhang et al. 2003), the enzyme forms an extended parallel β-sheet with the peptide backbone of H3, similar to the hSET8:histone H4 complex. However, the side chains of histone H3 participate in few contacts within the substrate-binding cleft of DIM-5, unlike the intimate series of interactions that are critical for histone H4 recognition by hSET8. Recent studies of the substrate specificity of hSET7/9 have revealed that it recognizes a consensus motif in its protein substrates: K/R-S/T-**K** (in which **K** is the methylation site) (Chuikov et al. 2004). Although hSET7/9 recognizes a specific series of residues preceding its methylation site, this PKMT does not form an extensive β-sheet with the protein substrate, unlike DIM-5 and hSET8. To summarize, the histone specificity of hSET8 appears to be a combination of the substrate-binding modes of DIM-5 and hSET7/9 in which the enzyme not only engages in an extended parallel β-sheet with H4, but also recognizes the residues flanking Lys-20 through an extensive network of side-chain interactions (Fig. 3B).

Product specificity of hSET8

Analyses of histone H4 Lys-20 methylation patterns in *Drosophila* and HeLa cells suggest that hSET8 functions as a monomethylase. However, the degree of methylation of Lys-20 catalyzed by this enzyme, commonly referred to as the product specificity of a PKMT (Zhang et al. 2003), has not been rigorously established. To determine the product specificity of hSET8, we conducted histone methyltransferase assays and subjected aliquots of the reaction to MALDI mass spectrometry to determine the methylation state of Lys-20 in histone H4. The data indicate a shift in the mass/charge (m/z) ratio from 1320 to 1334 in the H4 peptide after its reaction with hSET8, corresponding to the addition of a single methyl group (Fig. 4A). Incubation of the enzyme with the H4 peptide for 24 h results in a complete conversion to monomethyl-Lys-20 with no discernible accumulation of the di- or trimethylated states (data not shown). Thus, wild-type hSET8 is a bona fide histone H4 Lys-20 monomethylase, correlating with its in vivo function in maintaining Lys-20 monomethylation during cell division.

After characterizing the product specificity of hSET8, we sought to understand the mechanisms that control lysine monomethylation by this PKMT. Examination of the active site reveals two residues, Tyr-245 and Tyr-334, that hydrogen-bond to the ε-amino group of Lys-20 through direct and water-mediated interactions, respectively (Fig. 4B). The positions of the hydroxyl groups of these tyrosines are structurally conserved with Tyr-245 and Tyr-305, respectively, in the active site of hSET7/9 (Fig. 4C). The Tyr-245/Tyr-305 pair hydrogen-bonds to the ε-amino group of Lys-4 in histone H3 and arrests catalysis at the monomethylation state through stabilization of the methyllysine product complex in hSET7/9 (Fig. 4C; Xiao et al. 2003a; Zhang et al. 2003). The structural similarities of the lysine-binding channels of these
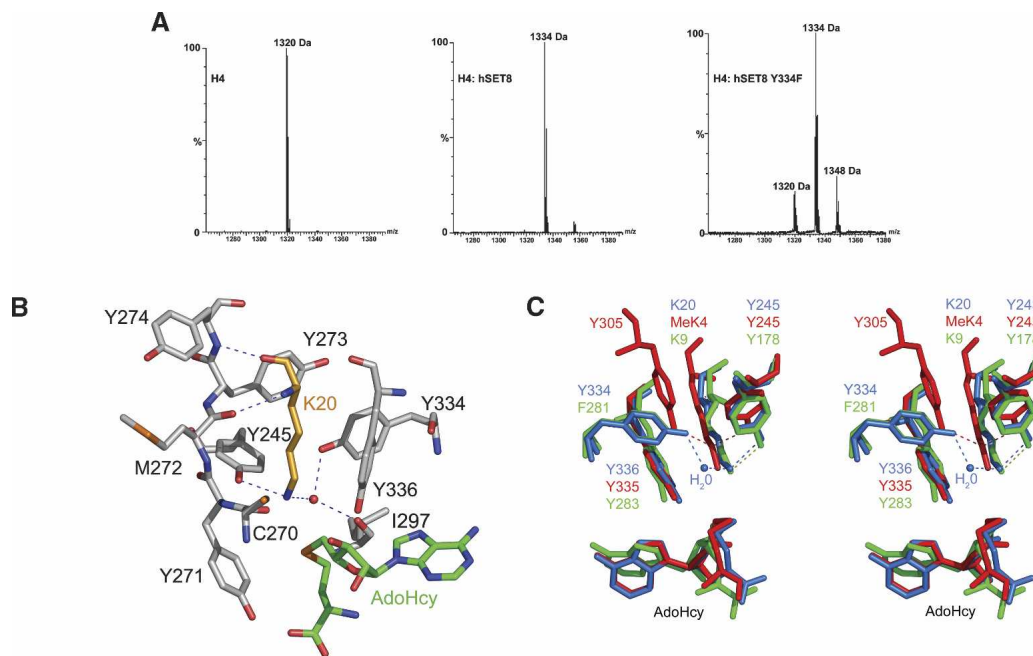

Figure 4. Product specificity of hSET8. (*A*) MALDI mass spectrometry of the 10-residue histone H4 peptide (m/z = 1320) and its methylation by wild-type hSET8 and the Y334F mutant. (*B*) Close-up view of hSET8 lysine-binding channel. Residues and the water molecule that interact with the side chain of Lys-20 are illustrated. Hydrogen bonds are rendered as dashed blue lines. The carbon atoms of Lys-20, AdoHcy, and the enzyme are depicted in gold, green, and gray, respectively. (*C*) Stereoview of a superimposition of the lysine-binding channels of hSET8:H4 Lys-20 (blue), hSET7/9:H3 MeLys4 (1O9S.pdb, red), and DIM-5:H3 Lys-9 (1PEG.pdb, green). Hydrogen bonds are rendered with dashed lines corresponding to the color of each enzyme.

Table 3. *Mutational analysis of the tyrosines within the lysine binding channel of hSET8*

Lysine pore	K_D (µM)	K_m (µM)	k_{cat} (min^{-1})	k_{cat}/K_m (µM^{-1} × min^{-1}) × 10^3
Wild type	33 ± 1	400 ± 30	0.43 ± 0.02	1.1 ± 0.1
Y245A	>500	N.A.	N.A.	N.A.
Y245F	>500	N.A.	N.A.	N.A.
Y334A	>500	—	—	0.005 ± 0.001
Y334F	19 ± 2	520 ± 30	0.45 ± 0.11	0.90 ± 0.20

(>500) A lower limit of the K_D value is reported because saturation of the enzyme with ligand could not be achieved during ITC titrations.
(N.A.) No activity was detected in the methyltransferase assay.
(—) The individual values of K_M and k_{cat} are not reported because the K_M value is beyond the measurable range; the k_{cat}/K_M values are reported in these cases.

two PKMTs provide a mechanistic explanation for the product specificity of hSET8. To further probe the methyltransfer properties of the enzyme, we superimposed its active site with DIM-5, a histone H3 Lys-9-specific methyltransferase (Fig. 4C). The alignment reveals that Tyr-245 in hSET8 is structurally conserved with Tyr-178 in DIM-5, whereas Tyr-334 aligns with a phenylalanine (Phe-281), respectively. The absence of a second hydrogen-bonding tyrosine in the active site of DIM-5 enables this PKMT to catalyze trimethylation of Lys-9 in H3 (Zhang et al. 2003). Based on this observation, we hypothesized that mutation of either Tyr-245 or Tyr-334 in the active site of hSET8 might convert the product specificity of this PKMT to either a Lys-20 di- or trimethylase.

To test this hypothesis, we mutated each of these tyrosines to alanine or phenylalanine, respectively, and determined the enzymatic activity and product specificity of each mutant. Mutation of Tyr-334 to phenylalanine has virtually no effect on histone H4 binding or methylation by hSET8, whereas an alanine substitution at this position severely compromises enzymatic activity (Table 3). Mass spectrometric analysis of the Y334F mutant reveals that it is capable of catalyzing mono- and dimethylation of Lys-20 in histone H4 (Fig. 4A). Reaction of the H4 peptide with the Y334F mutant for 24 h primarily yields dimethyl-Lys-20 with no detectable trimethylation of this residue (data not shown). These results are consistent with our prediction based on the active-site alignment with DIM-5 and also agree with the structurally homologous Y305F mutation in hSET7/9, which converts this PKMT to a histone H3 Lys-4 dimethylase (Fig. 4C; Zhang et al. 2003). In contrast, mutation of Tyr-245 to either alanine or phenylalanine completely abolishes methyltransfer by hSET8. The effects of these substitutions correlate with mutations of the structurally conserved Tyr-245 in hSET7/9 that disrupt the activity of this PKMT (Xiao et al. 2003a). Taken together, the mutational analysis of Tyr-245 and Tyr-334 in the active site of hSET8 provides a molecular basis for histone H4 Lys-20 monomethylation by this PKMT. Moreover, our results concur with the Phe/Tyr switch model recently proposed by Cheng and colleagues in which the presence or absence of specific tyrosines within the lysine-binding channel governs the product specificity of SET-domain PKMTs (Collins et al. 2005).

Conclusions

In summary, the biochemical and structural studies of hSET8 presented herein have elucidated the mechanisms by which this PKMT recognizes histone H4 Lys-20, permitting the identification of a consensus methylation motif for the enzyme. It will be interesting to determine whether other H4 Lys-20-specific methyltransferases, such as SUV4-20H1/2 (Schotta et al. 2004), exhibit a similar specificity for the residues that flank this lysine. In addition, our analysis of the product specificity of hSET8 has established that this enzyme is a Lys-20 monomethylase, in agreement with previous reports of histone H4 methylation in HeLa cells (Julien and Herr 2004) and *Drosophila* (Karachentsev et al. 2005). Despite the role of this PKMT in maintaining Lys-20 monomethylation during the cell cycle, the mechanisms by which this modification mediates transcriptional silencing are currently unresolved. Identifying effector proteins that specifically recognize the monomethylated state of Lys-20 will be pivotal in gaining a complete perspective of the regulatory functions of SET8 in mitosis and gene expression in metazoans.

Materials and methods

Cloning and expression of hSET8

A construct of hSET8 encoding residues 191–352 was cloned into the parallel expression vector pHIS2 using BamHI and XhoI restriction sites (Sheffield et al. 1999). The enzyme was then overexpressed in *Escherichia coli* BL21 (DE3) Codon Plus RIL cells (Stratagene) at 17°C and purified to homogeneity using Talon Co^{2+} (Clontech) affinity and Superdex 75 (Amersham Biosciences) gel filtration chromatographies, essentially as reported for pea Rubisco LSMT (Trievel et al. 2002) (with the exception that gel filtration was performed in 20 mM Tris-HCl at pH 7.0, 100 mM NaCl, and 10 mM β-mercaptoethanol). Mutants of hSET8 were prepared using the QuikChange Site-Directed Mutagenesis Kit (Stratagene), and the sequences were verified by dideoxy sequencing. Mutants of hSET8 were expressed and purified as described for the wild-type enzyme.

Histone H4 peptides

Wild-type and mutant histone H4 peptides (sequence: A_{15}-K_{16}-R_{17}-H_{18}-R_{19}-K_{20}-V_{21}-L_{22}-R_{23}-D_{24}) were purchased from New England Peptide, Inc. Peptides were synthesized with N-terminal

acetyl and C-terminal amide groups and were delivered as 2.5-mg lyophilized aliquots that were resuspended in deionized water to the appropriate concentration prior to use.

Crystallization and structure determination

Selenomethionyl-derivatized hSET8 containing an I220M mutation was prepared according to the protocol of Doublie (1997). Native and SeMet crystals of the ternary complex were obtained in 25%–35% Pentaerythritol Ethoxylate (15/4), 50 mM $(NH_4)_2SO_4$, and 100 mM Bis-TRIS (pH 6.0–7.0) at 4°C using 40 mg/mL hSET8 and a twofold molar ratio of the histone H4 peptide and AdoHcy. Crystals were then harvested in mother liquor and directly flash-frozen in liquid nitrogen. A selenomethionyl multiwavelength anomalous dispersion (MAD) experiment was conducted at the 32-ID beamline of COM-CAT at the Advanced Photon Source Synchrotron. Data were collected on a single crystal of the I220M mutant at the selenium edge with a Mar165 CCD detector (Mar Research) and subsequently processed and scaled using Denzo and Scalepack (Table 1; Otwinowski and Minor 1997). A complete high-resolution data set was also collected to 1.45 Å using a single crystal of native hSET8. After processing and scaling the peak, inflection point, and high remote wavelength data sets, the data were submitted for structure determination in the Automated Crystallographic System (ACrS) (Brunzelle et al. 2003). The best solution resulted from the HySS (Grosse-Kunstleve and Adams 2003), SHARP (de la Fortelle and Bricogne 1997), DM/Solomon (Cowtan and Main 1993; Abrahams and Leslie 1996), and ARP/wARP (Perrakis et al. 1999) pathway. The 2.0 Å experimental map was readily interpretable and permitted automated model building in ARP/wARP (Fig. 1A). The resulting hSET8 model was then used for molecular replacement with the native data set in MOLREP (Vagin and Teplyakov 1997). Four molecules were located in the triclinic cell, which were then used for model building in O (Jones et al. 1991) and refinement in REFMAC (Murshudov et al. 1997). In later stages of refinement, water molecules were added, and residues with alternative conformations were modeled. In the final model, Ala-15 and the side chain of Lys-16 were omitted due to poor electron density in the N terminus of the H4 peptide. The final structure has $R_{working}$ and R_{free} values of 16.9% and 19.9%, respectively (Table 1) and excellent geometry with none of the nonglycine residues present in the disallowed regions of the Ramachandran plot. Structural figures were generated and rendered in PyMOL (http://www.pymol.org).

Isothermal titration calorimetry

The equilibrium dissociation constants of wild type and mutants of hSET8 and histone H4 were determined using a VP-ITC calorimeter (MicroCal, LLC). The enthalpies of binding of wild type and mutants of hSET8 (60–120 µM) and the histone H4 peptide (1.0–2.0 mM) were measured at 20°C in 20 mM sodium phosphate (pH 7.0) and 100 mM NaCl. A saturating concentration of AdoHcy (1.0–2.0 mM) was used in all titrations. ITC data were subsequently analyzed using Origin 7.0 (OriginLab Corp.) with blank injections of ligand into buffer subtracted from the experimental titrations prior to data analysis. All of the calculated binding curves had *N*-values between 0.85 and 1.00. Curve-fitting errors for each experiment are reported in Tables 2 and 3.

Histone methyltransferase assays

The steady-state kinetic parameters for wild type and mutants of hSET8 and histone H4 were determined using a coupled fluorescent methyltransferase assay recently developed in our laboratory (Collazo et al. 2005). S-adenosylmethionine (AdoMet) was purified by cation exchange to remove impurities present in the commercially available cofactor, as described by Barker and coworkers (Chirpich et al. 1970). Assays were performed in 100 mM HEPES buffer (pH 7.5) and 0.02% maleimide-treated BSA with 0.5–2.0 µM hSET8, a saturating concentration of AdoMet (50 µM), and varying concentrations of histone H4 peptide. Assays were performed in duplicate with a final volume of 150 µL. To determine the K_M and k_{cat} values, peptide concentrations were varied from 0.05 to 4.0 mM. In cases in which the K_M value was too high to be accurately measured (>2.5 mM), the substrate specificity (k_{cat}/K_M) was determined by varying the H4 peptide concentration (0.16–0.64 mM) below the K_M value. This simplification permits the k_{cat}/K_M value to be determined from the linear relationship between the initial velocity and substrate concentration within this range of the Michaelis-Menten plot. Fluorescence was measured using a GeniosPro microplate reader (Tecan), and initial velocities were calculated by a linear fit from the plot of the fluorescence values versus time. The steady-state kinetics parameters were then calculated by plotting the velocity versus peptide concentration and fitting the Michaelis-Menten equation to the data in SigmaPlot (Systat Software, Inc.).

Mass spectrometry analysis

Histone methyltransferase assays were performed with wild-type hSET8 and the Tyr-245 and Tyr-334 mutants (5 µM) as described above and were quenched after 15 min or 24 h by the addition of 0.5% trifluoroacetic acid. Aliquots of the samples were cocrystallized with α-cyano-4-hydroxycinnamic acid (1:1), applied on the target, and dried at room temperature. The mass spectra were acquired on the TofSpec 2E MALDI-TOF mass spectrometer (Waters, Inc.) in reflectron mode, with each spectrum representing the average of 50 laser shots. Close external calibration was used based on the following mixture: bradikinin fragment 1–8, m/z = 904.41 (for [M + H]+); angiotensin II, m/z = 1046.54; [Glu1]-fibrinopeptide B, m/z = 1570.68; ACTH (clip 18–39), m/z = 2465.20.

References

Aasland, R., Abrams, C., Ampe, C., Ball, L.J., Bedford, M.T., Cesareni, G., Gimona, M., Hurley, J.H., Jarchau, T., Lehto, V.P., et al. 2002. Normalization of nomenclature for peptide motifs as ligands of modular protein domains. *FEBS Lett.* **513:** 141–144.

Abrahams, J.P. and Leslie, A.G.W. 1996. Methods used in the

structure determination of bovine mitochondrial F1 ATPase. *Acta Crystallogr. D Biol. Crystallogr.* **52:** 30–42.

Beisel, C., Imhof, A., Greene, J., Kremmer, E., and Sauer, F. 2002. Histone methylation by the *Drosophila* epigenetic transcriptional regulator Ash1. *Nature* **419:** 857–862.

Brunzelle, J.S., Shafaee, P., Yang, X., Weigand, S., Ren, Z., and Anderson, W.F. 2003. Automated crystallographic system for high-throughput protein structure determination. *Acta Crystallogr. D Biol. Crystallogr.* **59:** 1138–1144.

Chirpich, T.P., Zappia, V., Costilow, R.N., and Barker, H.A. 1970. Lysine 2,3-aminomutase. Purification and properties of a pyridoxal phosphate and S-adenosylmethionine-activated enzyme. *J. Biol. Chem.* **245:** 1778–1789.

Chuikov, S., Kurash, J.K., Wilson, J.R., Xiao, B., Justin, N., Ivanov, G.S., McKinney, K., Tempst, P., Prives, C., Gamblin, S.J., et al. 2004. Regulation of p53 activity through lysine methylation. *Nature* **432:** 353–360.

Collazo, E., Couture, J.-F., Bulfer, S., and Trievel, R.C. 2005. A coupled fluorescent assay for histone methyltransferases. *Anal. Biochem.* (in press).

Collins, R.E., Tachibana, M., Tamaru, H., Smith, K.M., Jia, D., Zhang, X., Selker, E.U., Shinkai, Y., and Cheng, X. 2005. In vitro and in vivo analyses of a Phe/Tyr switch controlling product specificity of histone lysine methyltransferases. *J. Biol. Chem.* **280:** 5563–5570.

Cowtan, K. and Main, P. 1993. Improvement of macromolecular electron density maps by the simultaneous application of real and reciprocal space constraints. *Acta Crystallogr. D Biol. Crystallogr.* **49:** 148–157.

de la Fortelle, E. and Bricogne, G. 1997. Maximum-likelihood heavy-atom parameter refinement for multiple isomorphous replacement and multiwavelength anomalous diffraction methods. *Methods Enzymol.* **276:** 474–492.

Doublie, S. 1997. Preparation of selenomethionyl proteins for phase determination. In *Methods in Enzymology* (eds. C.W. Carter and R.M. Sweet), pp. 523–530. Academic Press, New York.

Fang, J., Feng, Q., Ketel, C.S., Wang, H., Cao, R., Xia, L., Erdjument-Bromage, H., Tempst, P., Simon, J.A., and Zhang, Y. 2002. Purification and functional characterization of SET8, a nucleosomal histone H4-lysine 20-specific methyltransferase. *Curr. Biol.* **12:** 1086–1099.

Fischle, W., Wang, Y., and Allis, C.D. 2003. Histone and chromatin cross-talk. *Curr. Opin. Cell Biol.* **15:** 172–183.

Georgi, A.B., Stukenberg, P.T., and Kirschner, M.W. 2002. Timing of events in mitosis. *Curr. Biol.* **12:** 105–114.

Grosse-Kunstleve, R.W. and Adams, P.D. 2003. Substructure search procedures for macromolecular structures. *Acta Crystallogr. D Biol. Crystallogr.* **59:** 1966–1973.

Jones, T.A., Zou, J.Y., Cowan, S.W., and Kjeldgaard, M. 1991. Improved methods for building protein models in electron density maps and the location of errors in these models. *Acta Crystallogr. A* **47:** 110–119.

Julien, E. and Herr, W. 2004. A switch in mitotic histone H4 lysine 20 methylation status is linked to M phase defects upon loss of HCF-1. *Mol. Cell* **14:** 713–725.

Karachentsev, D., Sarma, K., Reinberg, D., and Steward, R. 2005. PR-Set7-dependent methylation of histone H4 Lys 20 functions in repression of gene expression and is essential for mitosis. *Genes & Dev.* **19:** 431–435.

Kuzmichev, A., Jenuwein, T., Tempst, P., and Reinberg, D. 2004. Different ezh2-containing complexes target methylation of histone H1 or nucleosomal histone H3. *Mol. Cell* **14:** 183–193.

Murshudov, G.N., Vagin, A.A., and Dodson, E.J. 1997. Refinement of macromolecular structures by the maximum-likelihood method. *Acta Cryst. D* **53:** 240–255.

Nishioka, K., Rice, J.C., Sarma, K., Erdjument-Bromage, H., Werner, J., Wang, Y., Chuikov, S., Valenzuela, P., Tempst, P., Steward, R., et al. 2002. PR-Set7 is a nucleosome-specific methyltransferase that modifies lysine 20 of histone H4 and is associated with silent chromatin. *Mol. Cell* **9:** 1201–1213.

Otwinowski, Z. and Minor, W. 1997. Processing of X-ray diffraction data collected in oscillation mode. *Methods Enzymol.* **276:** 307–326.

Perrakis, A., Morris, R., and Lamzin, V.S. 1999. Automated protein model building combined with iterative structure refinement. *Nat. Struct. Biol.* **6:** 458–463.

Rayasam, G.V., Wendling, O., Angrand, P.O., Mark, M., Niederreither, K., Song, L., Lerouge, T., Hager, G.L., Chambon, P., and Losson, R. 2003. NSD1 is essential for early post-implantation development and has a catalytically active SET domain. *EMBO J.* **22:** 3153–3163.

Rice, J.C., Nishioka, K., Sarma, K., Steward, R., Reinberg, D., and Allis, C.D. 2002. Mitotic-specific methylation of histone H4 Lys 20 follows increased PR-Set7 expression and its localization to mitotic chromosomes. *Genes & Dev.* **16:** 2225–2230.

Sanders, S.L., Portoso, M., Mata, J., Bahler, J., Allshire, R.C., and Kouzarides, T. 2004. Methylation of histone H4 lysine 20 controls recruitment of Crb2 to sites of DNA damage. *Cell* **119:** 603–614.

Sarg, B., Koutzamani, E., Helliger, W., Rundquist, I., and Lindner, H.H. 2002. Postsynthetic trimethylation of histone H4 at lysine 20 in mammalian tissues is associated with aging. *J. Biol. Chem.* **277:** 39195–39201.

Schotta, G., Lachner, M., Sarma, K., Ebert, A., Sengupta, R., Reuter, G., Reinberg, D., and Jenuwein, T. 2004. A silencing pathway to induce H3-K9 and H4-K20 trimethylation at constitutive heterochromatin. *Genes & Dev.* **18:** 1251–1262.

Sheffield, P., Garrard, S., and Derewenda, Z. 1999. Overcoming expression and purification problems of RhoGDI using a family of 'parallel' expression vectors. *Protein Expr. Purif.* **15:** 34–39.

Sims III, R.J., Nishioka, K., and Reinberg, D. 2003. Histone lysine methylation: A signature for chromatin function. *Trends Genet.* **19:** 629–639.

Trievel, R.C. 2004. Structure and function of histone methyltransferases. *Crit. Rev. Eukaryot. Gene Expr.* **14:** 147–170.

Trievel, R.C., Beach, B.M., Dirk, L.M., Houtz, R.L., and Hurley, J.H. 2002. Structure and catalytic mechanism of a SET domain protein methyltransferase. *Cell* **111:** 91–103.

Vagin, A. and Teplyakov, A. 1997. MOLREP: An automated program for molecular replacement. *J. Appl. Cryst.* **30:** 1022–1025.

Wilson, J.R., Jing, C., Walker, P.A., Martin, S.R., Howell, S.A., Blackburn, G.M., Gamblin, S.J., and Xiao, B. 2002. Crystal structure and functional analysis of the histone methyltransferase SET7/9. *Cell* **111:** 105–115.

Xiao, B., Jing, C., Wilson, J.R., Walker, P.A., Vasisht, N., Kelly, G., Howell, S., Taylor, I.A., Blackburn, G.M., and Gamblin, S.J. 2003a. Structure and catalytic mechanism of the human histone methyltransferase SET7/9. *Nature* **421:** 652–656.

Xiao, B., Wilson, J.R., and Gamblin, S.J. 2003b. SET domains and histone methylation. *Curr. Opin. Struct. Biol.* **13:** 699–705.

Zhang, X., Tamaru, H., Khan, S.I., Horton, J.R., Keefe, L.J., Selker, E.U., and Cheng, X. 2002. Structure of the *Neurospora* SET domain protein DIM-5, a histone H3 lysine methyltransferase. *Cell* **111:** 117–127.

Zhang, X., Yang, Z., Khan, S.I., Horton, J.R., Tamaru, H., Selker, E.U., and Cheng, X. 2003. Structural basis for the product specificity of histone lysine methyltransferases. *Mol. Cell* **12:** 177–185.